An improved complex variable element-free Galerkin method for two-dimensional elasticity problems*

Bai Fu-Nong(白福浓), Li Dong-Ming(李冬明) Wang Jian-Fei(王健菲), and Cheng Yu-Min(程玉民)†

[a] *Shanghai Institute of Applied Mathematics and Mechanics, Shanghai University, Shanghai* 200072, *China*

[b] *Shanghai Key Laboratory of Mechanics in Energy Engineering, Shanghai University, Shanghai* 200072, *China*

(Received 2 August 2011; revised manuscript received 19 August 2011)

In this paper, the improved complex variable moving least-squares (ICVMLS) approximation is presented. The ICVMLS approximation has an explicit physics meaning. Compared with the complex variable moving least-squares (CVMLS) approximations presented by Cheng and Ren, the ICVMLS approximation has a great computational precision and efficiency. Based on the element-free Galerkin (EFG) method and the ICVMLS approximation, the improved complex variable element-free Galerkin (ICVEFG) method is presented for two-dimensional elasticity problems, and the corresponding formulae are obtained. Compared with the conventional EFG method, the ICVEFG method has a great computational accuracy and efficiency. For the purpose of demonstration, three selected numerical examples are solved using the ICVEFG method.

Keywords: meshless method, improved complex variable moving least-squares approximation, improved complex variable element-free Galerkin method, elasticity

PACS: 02.60.Cb, 02.60.Lj, 46.25.–y **DOI:** 10.1088/1674-1056/21/2/020204

1. Introduction

In recent years, meshless methods have been successfully developed and used to solve a variety of science and engineering problems.[1−7] Some traditional numerical methods, such as the finite element method (FEM) and the boundary element method (BEM), are very successful methods for science and engineering problems, but they cannot be effectively applied to some complicated problems, such as extremely large deformation and crack growth problems.[1,2] The meshless method, which is based on nodes with a minimum of meshing or no meshing at all, can solve many engineering problems that are not suited to conventional computational methods. The meshless method has shown some advantages over traditional numerical methods.[1,3]

The moving least-squares (MLS) approximation,[8] which is most widely used, is one of the methods used to form the shape function in the meshless method. The shape function that is formed with the MLS approximation is able to obtain a very accurate solution. However, the MLS approximation is the approximation of a scalar function, and thus the meshless method that is derived from it requires a lot of nodes in the domain.[9,10]

To overcome the above disadvantage of the MLS approximation, the complex variable moving least-squares (CVMLS) approximation has been developed.[9−15] The CVMLS approximation is the approximation of a vector function, and with this approximation, the trial function of a two-dimensional problem is formed with a one-dimensional basis function. The number of unknown coefficients in the trial function of the CVMLS approximation is less than that in the trial function of the MLS approximation, and we can thus select fewer nodes in the meshless method that is formed from the CVMLS approximation than those required in the meshless method of the MLS approximation with no loss of accuracy. The meshless method that is derived from the CVMLS approximation also has a greater computational efficiency.

In the CVMLS approximation, the mathematical and the physical meanings of the functional are not clear. Then, based on the CVMLS approximation, a new complex variable moving least-squares approximation has been developed,[16] in which the functional

*Project supported by the National Natural Science Foundation of China (Grant No. 11026223), the Shanghai Leading Academic Discipline Project, China (Grant No. S30106), and the Innovation Fund Project for Graduate Student of Shanghai University, China (Grant No. SHUCX112359).

†Corresponding author. E-mail: ymcheng@shu.edu.cn

© 2012 Chinese Physical Society and IOP Publishing Ltd

has an explicit physics meaning.

In this paper, the improved complex variable moving least-squares (ICVMLS) approximation is presented. The ICVMLS approximation has an explicit physics meaning. Compared with the complex variable moving least-squares (CVMLS) approximations presented by Cheng and Ren, the ICVMLS approximation has a great computational accuracy and efficiency. Based on the element-free Galerkin (EFG) method[17,18] and the ICVMLS approximation, the improved complex variable element-free Galerkin (ICVEFG) method is presented for two-dimensional elasticity problems, and the corresponding formulae are obtained. Compared with conventional EFG methods, the ICVEFG method has a great computational accuracy and efficiency. For the purposes of demonstration, three selected numerical examples are solved using the ICVEFG method.

2. Improved complex variable moving least-squares approximation

Similar to the CVMLS approximation, the ICVMLS approximation is also an approximation of a vector function.

In the ICVMLS approximation, the trial function is

$$\begin{aligned} u^h(z) &= u_1^h(z) + \mathrm{i}\, u_2^h(z) \\ &= \sum_{i=1}^{m} \bar{p}_i(z) a_i(z) = \bar{\boldsymbol{p}}^{\mathrm{T}}(z)\boldsymbol{a}(z), \\ z &= x_1 + \mathrm{i}\, x_2 \in \Omega, \end{aligned} \tag{1}$$

where $u^h(z)$ is the approximation of function $u(z)$, $\bar{\boldsymbol{p}}^{\mathrm{T}}(z) = (\bar{p}_1(z), \bar{p}_2(z), \ldots, \bar{p}_m(z))$ is the basis function vector which equals the conjugate of the basis function vector $\boldsymbol{p}^{\mathrm{T}}(z) = (p_1(z), p_2(z), \ldots, p_m(z))$, $\boldsymbol{a}^{\mathrm{T}}(z) = (a_1(z), a_2(z), \ldots, a_m(z))$ is the corresponding coefficient vector, and m is the number of terms in the basis function.

The local approximation at point z is defined as

$$u^h(z, \hat{z}) = \sum_{i=1}^{m} \bar{p}_i(z) \cdot a_i(z, \hat{z}) = \bar{\boldsymbol{p}}^{\mathrm{T}}(z) \cdot \boldsymbol{a}(z, \hat{z}), \tag{2}$$

where $\hat{z}$ is the node in the local domain of z.

Define a functional

$$\begin{aligned} J &= \sum_{I=1}^{n} w(z - z_I) \left| u^h(z_I, z) - u(z_I) \right|^2 \\ &= \sum_{I=1}^{n} w(z - z_I) \big(u^h(z_I, z) - u(z_I)\big) \\ &\quad \times \big(\overline{u^h(z_I, z) - u(z_I)}\big) \\ &= \sum_{I=1}^{n} w(z - z_I) \Big(\sum_{i=1}^{m} \bar{p}_i(z_I) \cdot a_i(z, \hat{z}) - u(z_I)\Big) \\ &\quad \times \Big(\overline{\sum_{i=1}^{m} \bar{p}_i(z_I) \cdot a_i(z, \hat{z}) - u(z_I)}\Big), \end{aligned} \tag{3}$$

where $w(z - z_I)$ is a weighting function with compact support, and z_I $(I = 1, 2, \ldots, n)$ are the nodes with domains of influence which cover point z.

Define inner product

$$\begin{aligned} (f, g)_z &= \sum_{I=1}^{n} w(z - z_I) f(z_I) \bar{g}(z_I), \\ &\qquad \forall f, g \in C^0(\bar{\Omega}), \end{aligned} \tag{4}$$

where $\bar{g}(z_I)$ is the conjugate of $g(z_I)$, $\bar{\Omega} = \Omega \cup \partial\Omega$, and $C^0(\bar{\Omega})$ is the set of all continuous functions in the domain $\bar{\Omega}$. And the corresponding norm at z is of course

$$\|f\|_z = [(f, f)_z]^{1/2}. \tag{5}$$

Equation (3) can be written as

$$\begin{aligned} J &= (\bar{\boldsymbol{P}}\boldsymbol{a}(z, \hat{z}) - \boldsymbol{u}(\hat{z}))^{\mathrm{T}} \boldsymbol{W}(z, \hat{z}) (\overline{\bar{\boldsymbol{P}}\boldsymbol{a}(z, \hat{z}) - \boldsymbol{u}(\hat{z})}) \\ &= \left\| \bar{\boldsymbol{p}}^{\mathrm{T}}(z) \cdot \boldsymbol{a}(z, \hat{z}) - u \right\|_z^2, \end{aligned} \tag{6}$$

$$\boldsymbol{u}(\hat{z}) = (u(z_1), u(z_2), \ldots, u(z_n))^{\mathrm{T}} = \boldsymbol{Q}\boldsymbol{u}, \tag{7}$$

$$\begin{aligned} \boldsymbol{u} = \big(&u_1(z_1), u_2(z_1), u_1(z_2), u_2(z_2), \ldots, \\ &u_1(z_n), u_2(z_n)\big)^{\mathrm{T}}, \end{aligned} \tag{8}$$

$$\boldsymbol{Q} = \begin{bmatrix} 1 & \mathrm{i} & 0 & 0 & 0 & 0 & \cdots & 0 & 0 \\ 0 & 0 & 1 & \mathrm{i} & 0 & 0 & \cdots & 0 & 0 \\ 0 & 0 & 0 & 0 & 1 & \mathrm{i} & \cdots & 0 & 0 \\ \vdots & \vdots & \vdots & \vdots & \vdots & \vdots & \ddots & \vdots & \vdots \\ 0 & 0 & 0 & 0 & 0 & 0 & \cdots & 1 & \mathrm{i} \end{bmatrix}_{n \times 2n}, \tag{9}$$

$$\boldsymbol{P} = \begin{bmatrix} p_1(z_1) & p_2(z_1) & \cdots & p_m(z_1) \\ p_1(z_2) & p_2(z_2) & \cdots & p_m(z_2) \\ \vdots & \vdots & \ddots & \vdots \\ p_1(z_n) & p_2(z_n) & \cdots & p_m(z_n) \end{bmatrix}_{n \times m}, \tag{10}$$

$$\bar{\boldsymbol{P}} = \begin{bmatrix} \bar{p}_1(z_1) & \bar{p}_2(z_1) & \cdots & \bar{p}_m(z_1) \\ \bar{p}_1(z_2) & \bar{p}_2(z_2) & \cdots & \bar{p}_m(z_2) \\ \vdots & \vdots & \ddots & \vdots \\ \bar{p}_1(z_n) & \bar{p}_2(z_n) & \cdots & \bar{p}_m(z_n) \end{bmatrix}_{n \times m}, \tag{11}$$

$$\begin{aligned} \boldsymbol{a}^{\mathrm{T}}(z, \hat{z}) &= (a_1(z, \hat{z}), a_2(z, \hat{z}), \ldots, a_m(z, \hat{z})) \\ &= (a_1, a_2, \ldots, a_m), \end{aligned} \tag{12}$$

$$\boldsymbol{W}(z,\hat{z}) = \begin{bmatrix} w(z-z_1) & 0 & \cdots & 0 \\ 0 & w(z-z_2) & \cdots & 0 \\ \vdots & \vdots & \ddots & \vdots \\ 0 & 0 & \cdots & w(z-z_n) \end{bmatrix}_{n\times n}. \tag{13}$$

Equation (3) can also be written as

$$J = \|a_1\bar{p}_1 + a_2\bar{p}_2 + \cdots + a_m\bar{p}_m - u\|_z^2, \tag{14}$$

where $\bar{p}_i = \bar{p}_i(z)$, $i = 1, 2, \ldots, m$.

Then let $u^{(1)}$ be the projection of u in the span $(\bar{p}_1, \bar{p}_2, \ldots, \bar{p}_m)$, obviously

$$J^{(1)} = \left\|u^{(1)} - u\right\|_z^2 \tag{15}$$

is the minimum of the functional J.

The function u could be written as

$$u = u^{(1)} + u^{(2)}, \tag{16}$$

where $u^{(2)} \perp \text{span}\,(\bar{p}_1, \bar{p}_2, \ldots, \bar{p}_m)$.

Obviously,

$$\left(\bar{p}_i, u^{(2)}\right)_z = 0, \quad (i = 1, 2, \ldots, m), \tag{17}$$

then, we have

$$\begin{aligned}(\bar{p}_i, u)_z &= (\bar{p}_i, u^{(1)})_z + (\bar{p}_i, u^{(2)})_z \\ &= (\bar{p}_i, u^{(1)})_z, \quad (i = 1, 2, \ldots, m).\end{aligned} \tag{18}$$

Equation (18) can be written as

$$\begin{aligned}(\bar{p}_i, u)_z &= (\bar{p}_i, u^{(1)})_z \\ &= (\bar{p}_i, a_1\bar{p}_1 + a_2\bar{p}_2 + \cdots + a_m\bar{p}_m)_z,\end{aligned} \tag{19}$$

then, we have

$$\begin{bmatrix} (\bar{p}_1,\bar{p}_1)_z & (\bar{p}_1,\bar{p}_2)_z & \cdots & (\bar{p}_1,\bar{p}_m)_z \\ (\bar{p}_2,\bar{p}_1)_z & (\bar{p}_2,\bar{p}_2)_z & \cdots & (\bar{p}_2,\bar{p}_m)_z \\ \vdots & \vdots & \ddots & \vdots \\ (\bar{p}_m,\bar{p}_1)_z & (\bar{p}_m,\bar{p}_2)_z & \cdots & (\bar{p}_m,\bar{p}_m)_z \end{bmatrix} \begin{bmatrix} \bar{a}_1(z,\hat{z}) \\ \bar{a}_2(z,\hat{z}) \\ \vdots \\ \bar{a}_m(z,\hat{z}) \end{bmatrix}$$

$$= \begin{bmatrix} (\bar{p}_1, u)_z \\ (\bar{p}_2, u)_z \\ \vdots \\ (\bar{p}_m, u)_z \end{bmatrix}. \tag{20}$$

Equation (20) can be written as

$$(\bar{\boldsymbol{P}}^{\mathrm{T}}\boldsymbol{W}(z,\hat{z})\boldsymbol{P})\bar{\boldsymbol{a}}(z,\hat{z}) = \bar{\boldsymbol{P}}^{\mathrm{T}}\boldsymbol{W}(z,\hat{z})\bar{\boldsymbol{u}}(\hat{z}), \tag{21}$$

and the conjugate of Eq. (21) can be written as

$$(\boldsymbol{P}^{\mathrm{T}}\boldsymbol{W}(z,\hat{z})\bar{\boldsymbol{P}})\boldsymbol{a}(z,\hat{z}) = \boldsymbol{P}^{\mathrm{T}}\boldsymbol{W}(z,\hat{z})\boldsymbol{u}(\hat{z}), \tag{22}$$

then we have

$$\boldsymbol{a}(z,\hat{z}) = \boldsymbol{A}^{-1}(z,\hat{z})\boldsymbol{B}(z,\hat{z})\boldsymbol{u}(\hat{z}), \tag{23}$$

where

$$\boldsymbol{A}(z,\hat{z}) = \boldsymbol{P}^{\mathrm{T}}\boldsymbol{W}(z,\hat{z})\bar{\boldsymbol{P}}, \tag{24}$$

$$\boldsymbol{B}(z,\hat{z}) = \boldsymbol{P}^{\mathrm{T}}\boldsymbol{W}(z,\hat{z}). \tag{25}$$

The expression of the local approximation $u^h(z,\hat{z})$ is

$$u^h(z,\hat{z}) = \boldsymbol{\Phi}(z)\boldsymbol{u}(\hat{z}) = \sum_{I=1}^{n}\Phi_I(z)u(z_I), \tag{26}$$

where $\boldsymbol{\Phi}(z)$ is called the shape function and

$$\begin{aligned}\boldsymbol{\Phi}(z) &= (\Phi_1(z), \Phi_2(z), \ldots, \Phi_n(z)) \\ &= \bar{\boldsymbol{p}}^{\mathrm{T}}(z)\boldsymbol{A}^{-1}(z,\hat{z})\boldsymbol{B}(z,\hat{z}).\end{aligned} \tag{27}$$

From Eq. (26) we have

$$u_1^h(z) = \mathrm{Re}\Big[\boldsymbol{\Phi}(z)\boldsymbol{u}(\hat{z})\Big] = \mathrm{Re}\Big[\sum_{I=1}^{n}\Phi_I(z)u(z_I)\Big], \tag{28}$$

$$u_2^h(z) = \mathrm{Im}\Big[\boldsymbol{\Phi}(z)\boldsymbol{u}(\hat{z})\Big] = \mathrm{Im}\Big[\sum_{I=1}^{n}\Phi_I(z)u(z_I)\Big]. \tag{29}$$

This is the ICVMLS approximation.

The ICVMLS approximation presented in this paper has all advantages of the CVMLS approximation. In the ICVMLS approximation, the trial function of a two-dimensional problem is formed with a one-dimensional basis function. Then the number of unknown coefficients in the trial function of the ICVMLS approximation is less than that in the trial function of the MLS approximation. In the MLS approximation, the linear basis is $\boldsymbol{p}^{\mathrm{T}} = (1, x_1, x_2)$, and three unknown coefficients are included in the trial function (1), whereas in the ICVMLS approximation, the linear basis is $\bar{\boldsymbol{p}}^{\mathrm{T}} = (1, \bar{z})$, and two unknown coefficients are included in the trial function (1). In the MLS approximation, the quadratic basis is $\boldsymbol{p}^{\mathrm{T}} = (1, x_1, x_2, x_1^2, x_1x_2, x_2^2)$, and six unknown coefficients are included in the trial function (1), whereas in the ICVMLS approximation, the quadratic basis is $\bar{\boldsymbol{p}}^{\mathrm{T}} = (1, \bar{z}, \bar{z}^2)$, and three unknown coefficients are included in the trial function (1). For an arbitrary point in the domain, we need fewer nodes with domains of influence which cover the point, and thus we also require fewer nodes in the whole domain.

Compared with the case in the CVMLS approximation, the functional J in the ICVMLS approximation has an explicit physics meaning.

Compared with the case in another CVMLS approximation presented in Ref. [16], in the ICVMLS approximation, the conjugate of the polynomial basis function is used to obtain high computational accuracy and efficiency. Thus the meshless method that

is derived from the ICVMLS approximation will also have higher computational accuracy and efficiency.

We will give an example to show the advantages of the ICVMLS approximation. Let

$$u_1(x_1,x_2)=\Big(1-\frac{x_1}{2}\Big)x_1x_2+\frac{1}{2}x_2^3-x_2,$$

$$u_2(x_1,x_2)=-\frac{1}{2}\Big[(1-x_1)x_2^2+\Big(1-\frac{x_1}{3}\Big)x_1^2\Big]-x_1.$$

And 441 nodes (x_{1i},x_{2j}), where

$$x_{1i}=0.1\times i-0.1,$$

$$x_{2j}=0.1\times j-0.1,\ (i,j=1,2,\ldots,21),$$

are selected. Then we calculate twenty thousand and one approximate values of the functions and their derivatives for points (p_i,q_i) $(i=1,2,\ldots,20001)$, where $p_i=0.45$, $q_i=0.0001\times \mathrm{i}-0.0001$. We find the CPU time that the ICVMLS approximation takes is 41.0519 s, and the one that the CVMLS approximation presented in Ref. [16] took was 42.6279 s. The approximate values of u_1 and u_2 of the ICVMLS approximation and the CVMLS approximation presented in Ref. [16] are shown in Fig. 1 and Fig. 2 respectively, and we find the function approximation values of the ICVMLS approximation and the CVMLS approximation are both close to the analytical values. However, the approximate value of the derivative $u_{1,1}$ of the ICVMLS approximation has less error than that of the CVMLS approximation (see Fig. 3), and the approximate value of the derivative $u_{2,2}$, especially near the boundary, of the ICVMLS approximation also has less error than that by the CVMLS approximation (see Fig. 4 and Table 1). Thus the ICVMLS approximation has a greater accuracy and computational efficiency than the CVMLS approximation presented in Ref. [16].

Table 1. Approximate values of function $u_{2,2}$ near the boundary.

Node coordinate	Analytical	ICVMLS	CVMLS
(0.45, 1.9991)	−1.0995	−1.07865	−0.107872
(0.45, 1.9992)	−1.09956	−1.07869	−0.10669
(0.45, 1.9993)	−1.09962	−1.07872	−0.105507
(0.45, 1.9994)	−1.09967	−1.07876	−0.104323
(0.45, 1.9995)	−1.09973	−1.0788	−0.103138
(0.45, 1.9996)	−1.09978	−1.07883	−0.101952
(0.45, 1.9997)	−1.09984	−1.07887	−0.100765
(0.45, 1.9998)	−1.09989	−1.0789	−0.0995769
(0.45, 1.9999)	−1.09994	−1.07894	−0.104323
(0.45, 2.0000)	−1.1	−1.07898	−0.103138

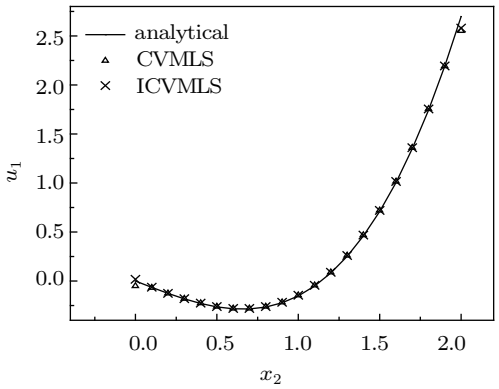


Fig. 1. Function u_1 at $x_1=0.45$.

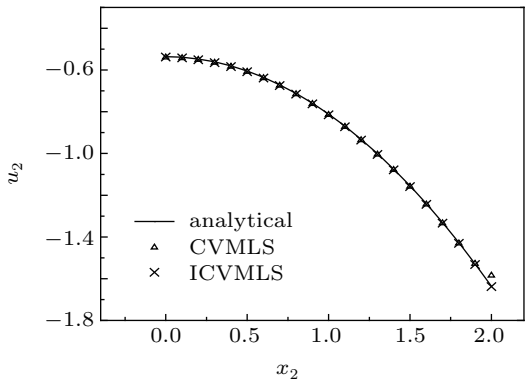


Fig. 2. Function u_2 at $x_1=0.45$.

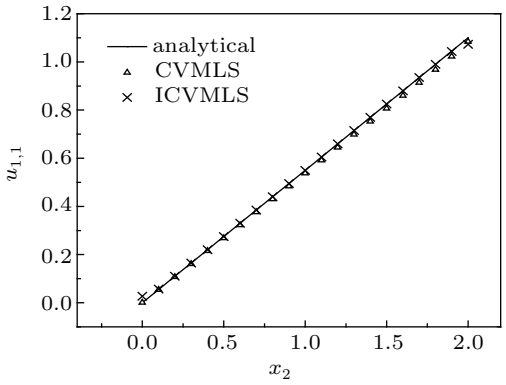


Fig. 3. Function $u_{1,1}$ at $x_1=0.45$.

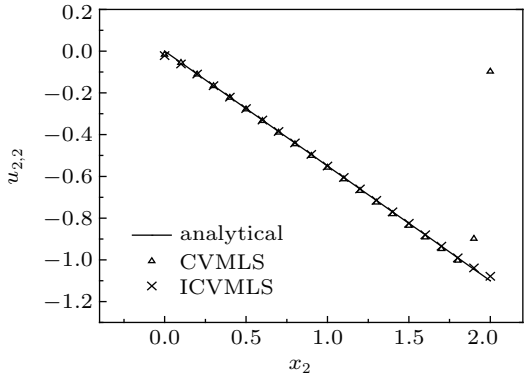


Fig. 4. Function $u_{2,2}$ at $x_1=0.45$.

3. Improved complex variable element-free Galerkin method for two-dimensional elasticity problems

According to the ICVMLS approximation and the EFG method, we propose an improved complex variable element-free Galerkin (ICVEFG) method for two-dimensional elasticity problems as follows.

From the approximation function (26), the displacement at an arbitrary point $z = x_1 + \mathrm{i}x_2$ in the domain can be expressed as

$$\begin{aligned} u(z) &= u_1(z) + \mathrm{i}\, u_2(z) = \boldsymbol{\Phi}(z)\boldsymbol{u}(\hat{z}) \\ &= \sum_{I=1}^{n} \Phi_I(z) u(z_I), \end{aligned} \tag{30}$$

i.e.,

$$u_1(z) = \mathrm{Re}[\boldsymbol{\Phi}(z)\boldsymbol{u}(\hat{z})] = \mathrm{Re}\Big[\sum_{I=1}^{n} \Phi_I(z) u(z_I)\Big], \tag{31}$$

$$u_2(z) = \mathrm{Im}[\boldsymbol{\Phi}(z)\boldsymbol{u}(\hat{z})] = \mathrm{Im}\Big[\sum_{I=1}^{n} \Phi_I(z) u(z_I)\Big]. \tag{32}$$

The strain tensor $\varepsilon(z)$ is

$$\varepsilon(z) = \begin{bmatrix} \Big(\mathrm{Re}\Big[\sum\limits_{I=1}^{n} \Phi_I(z) u(z_I)\Big]\Big)_{,1} \\ \Big(\mathrm{Im}\Big[\sum\limits_{I=1}^{n} \Phi_I(z) u(z_I)\Big]\Big)_{,2} \\ \Big(\mathrm{Re}\Big[\sum\limits_{I=1}^{n} \Phi_I(z) u(z_I)\Big]\Big)_{,2} + \Big(\mathrm{Im}\Big[\sum\limits_{I=1}^{n} \Phi_I(z) u(z_I)\Big]\Big)_{,1} \end{bmatrix}, \tag{33}$$

i.e.,

$$\varepsilon(z) = \begin{bmatrix} \mathrm{Re}\Big[\sum\limits_{I=1}^{n} \Phi_{I,1}(z) u(z_I)\Big] \\ \mathrm{Im}\Big[\sum\limits_{I=1}^{n} \Phi_{I,2}(z) u(z_I)\Big] \\ \mathrm{Re}\Big[\sum\limits_{I=1}^{n} \Phi_{I,2}(z) u(z_I)\Big] + \mathrm{Im}\Big[\sum\limits_{I=1}^{n} \Phi_{I,1}(z) u(z_I)\Big] \end{bmatrix}. \tag{34}$$

The strain tensor $\varepsilon(z)$ can then be expressed as

$$\varepsilon(z) = Lu(z), \tag{35}$$

where

$$L(\cdot) = \begin{bmatrix} (\mathrm{Re}[\cdot])_{,1} \\ (\mathrm{Im}[\cdot])_{,2} \\ (\mathrm{Re}[\cdot])_{,2} + (\mathrm{Im}[\cdot])_{,1} \end{bmatrix}. \tag{36}$$

From Eqs. (7) and (26) we have

$$\varepsilon(z) = \boldsymbol{L}(\boldsymbol{\Phi}(z)\boldsymbol{u}(\hat{z})) = \boldsymbol{L}(\boldsymbol{\Phi}(z)\boldsymbol{Q}\boldsymbol{u}) = \boldsymbol{B}(z) \cdot \boldsymbol{u}, \tag{37}$$

where

$$\boldsymbol{B}(z) = (\boldsymbol{B}_1(z), \boldsymbol{B}_2(z), \ldots, \boldsymbol{B}_n(z)), \tag{38}$$

$$\boldsymbol{B}_i(z) = \begin{bmatrix} \mathrm{Re}[\Phi_{i,1}(z)] & -\mathrm{Im}[\Phi_{i,1}(z)] \\ \mathrm{Im}[\Phi_{i,2}(z)] & \mathrm{Re}[\Phi_{i,2}(z)] \\ \mathrm{Re}[\Phi_{i,2}(x)] + \mathrm{Im}[\Phi_{i,1}(z)] & -\mathrm{Im}[\Phi_{i,2}(z)] + \mathrm{Re}[\Phi_{i,1}(z)] \end{bmatrix}. \tag{39}$$

The stress tensor $\boldsymbol{\sigma}(z)$ can then be expressed as

$$\boldsymbol{\sigma}(z) = \boldsymbol{D} \cdot \varepsilon(z) = \boldsymbol{D} \cdot \boldsymbol{B}(z) \cdot \boldsymbol{u}, \tag{40}$$

where

$$\boldsymbol{D} = \frac{E}{1-\nu^2} \begin{bmatrix} 1 & \nu & 0 \\ \nu & 1 & 0 \\ 0 & 0 & (1-\nu)/2 \end{bmatrix} \tag{41}$$

for a plain stress problem, and

$$\boldsymbol{D} = \frac{E}{(1+\nu)(1-2\nu)} \begin{bmatrix} 1-\nu & \nu & 0 \\ \nu & 1-\nu & 0 \\ 0 & 0 & (1-2\nu)/2 \end{bmatrix} \tag{42}$$

for a plain strain problem, E is the Young's modulus, and ν is the Poisson's ratio.

Consider the following two-dimensional problem on the domain Ω bounded by Γ:

$$\nabla \cdot \boldsymbol{\sigma} + \boldsymbol{b} = 0, \quad \text{in} \quad \Omega, \tag{43}$$

where $\boldsymbol{b}$ is the body force vector.

The corresponding boundary conditions are

$$\boldsymbol{u} = \boldsymbol{u}_0, \quad \text{on} \quad \Gamma_u, \tag{44}$$

$$\boldsymbol{t} = \boldsymbol{\sigma} \cdot \boldsymbol{n} = \boldsymbol{t}_0, \quad \text{on} \quad \Gamma_\sigma, \tag{45}$$

where $\boldsymbol{t}$ is the traction vector, $\boldsymbol{u}_0$ and $\boldsymbol{t}_0$ are the prescribed displacement and traction vectors on the displacement boundary Γ_u and on the traction boundary Γ_σ, respectively, and $\boldsymbol{n}$ is the unit vector outward normal to the boundary Γ.

The Galerkin weak form of Eqs. (43)–(45) is

$$\int_\Omega \boldsymbol{\sigma}^{\mathrm{T}} \delta\varepsilon \,\mathrm{d}\Omega - \int_\Omega \boldsymbol{b}^{\mathrm{T}} \delta u \,\mathrm{d}\Omega - \int_{\Gamma_\sigma} \boldsymbol{t}^{\mathrm{T}} \delta u \,\mathrm{d}\Gamma - \delta W_u = 0, \tag{46}$$

where δ is the variational operator, and δW_u represents a term that is introduced to enforce the essential boundary conditions. The explicit form of δW_u depends on the method by which the essential boundary conditions are applied, and the different discrete equations of Eq. (46) will be obtained as follows.

When the essential boundary conditions are applied with a penalty method, δW_u is defined as

$$\delta W_u = \alpha \int_{\Gamma_u} \delta \boldsymbol{u}^{\mathrm{T}} (\boldsymbol{u} - \boldsymbol{u}_0) \,\mathrm{d}\Gamma, \tag{47}$$

where α is the penalty factor which is a function of coordinates. To impose the boundary conditions completely, the penalty factor must be infinite, which is not possible in practical numerical analysis. In general, the use of a large positive number of the penalty factor will enforce the boundary conditions. In this paper, when

$$\alpha = 1.0 \times 10^{2\sim5} E, \tag{48}$$

the solution will have a good accuracy.

Substituting Eqs. (30), (37), (40), and (47) into Eq. (46) yields

$$(\boldsymbol{K} + \boldsymbol{G})\boldsymbol{u} = F + \boldsymbol{q}, \tag{49}$$

where

$$\boldsymbol{K} = \int_\Omega \boldsymbol{B}^{\mathrm{T}} \boldsymbol{D} \boldsymbol{B} \,\mathrm{d}\Omega, \tag{50}$$

$$\boldsymbol{F} = \int_\Omega \tilde{\boldsymbol{\Phi}}^{\mathrm{T}} \boldsymbol{b} \,\mathrm{d}\Omega + \int_{\Gamma_\sigma} \tilde{\boldsymbol{\Phi}}^{\mathrm{T}} \boldsymbol{t}_0 \,\mathrm{d}\Gamma, \tag{51}$$

$$\boldsymbol{G} = \alpha \int_{\Gamma_u} \tilde{\boldsymbol{\Phi}}^{\mathrm{T}} S \tilde{\boldsymbol{\Phi}} \,\mathrm{d}\Gamma, \tag{52}$$

$$\boldsymbol{q} = \alpha \int_{\Gamma_u} \tilde{\boldsymbol{\Phi}}^{\mathrm{T}} S \boldsymbol{u}_0 \,\mathrm{d}\Gamma, \tag{53}$$

and

$$\tilde{\boldsymbol{\Phi}}(z) = (\tilde{\boldsymbol{\Phi}}_I(z), \tilde{\boldsymbol{\Phi}}_I(z), \ldots, \tilde{\boldsymbol{\Phi}}_n(z)), \tag{54}$$

$$\tilde{\boldsymbol{\Phi}}_I(z) = \begin{bmatrix} \mathrm{Re}\,[\Phi_I(z)] & -\mathrm{Im}\,[\Phi_I(z)] \\ \mathrm{Im}\,[\Phi_I(z)] & \mathrm{Re}\,[\Phi_I(z)] \end{bmatrix}, \tag{55}$$

$$S = \begin{bmatrix} s_1 & 0 \\ 0 & s_2 \end{bmatrix}, \tag{56}$$

$$s_i = \begin{cases} 1, \text{if } u_i \text{ is the prescribed displacement on } \Gamma_u \\ \quad i = 1, 2; \\ 0, \text{if } u_i \text{ is not the prescribed displacement on} \\ \Gamma_u \quad i = 1, 2. \end{cases} \tag{57}$$

Then the improved complex variable element-free Galerkin (ICVEFG) method is presented.

4. Numerical examples

Three examples solved with the ICVEFG method are presented in this section. The node distribution for each example is regular. And the linear basis function and the cubic spline weight function are used.

The first example is for the Timoshenko beam subjected to traction at the free end as shown in Fig. 5. The beam has a length of L, height D, and its width is unit width, then the beam is assumed to be in a state of plane stress. The analytical displacements for this problem are given as[19]

$$u_1 = -\frac{px_2}{6EI}\Big[(6L - 3x_1)x_1 + (2+\nu)\big[x_2^2 - \frac{D^2}{4}\big]\Big], \tag{58}$$

$$u_2 = \frac{p}{6EI}\Big[3\nu(L - x_1)x_2^2 + (4+5\nu)\frac{D^2 x_1}{4} + (3L - x_1)x_1^2\Big], \tag{59}$$

where the moment of inertia I of the beam is given by

$$I = \frac{D^3}{12}. \tag{60}$$

The corresponding stresses are

$$\sigma_{11} = -\frac{p(L-x_1)x_2}{I}, \tag{61}$$

$$\sigma_{22} = 0, \tag{62}$$

$$\sigma_{12} = \frac{p}{2I}\Big[\frac{D^2}{4} - x_2^2\Big]. \tag{63}$$

The problem is solved for the plane stress case with $E = 3.0 \times 10^7$ Pa, $v = 0.4$, $L = 48$ m, $D = 12$ m, and $p = 1000$ N.

The node distribution in the domain is shown in Fig. 6, and 11×5 nodes are selected. And the essential boundary conditions are applied with the penalty method and the penalty factor $\alpha = 1.0 \times 10^2 E$.

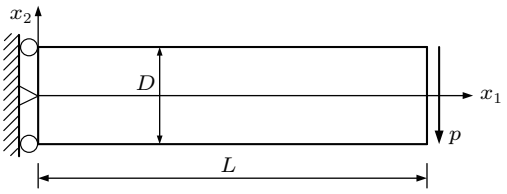


Fig. 5. A cantilever beam.

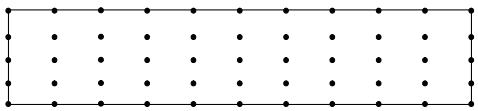


Fig. 6. Node distribution of the cantilever beam.

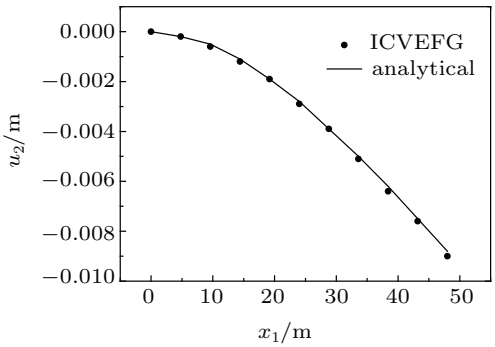


Fig. 7. Displacement u_2 at $x_2 = 0$.

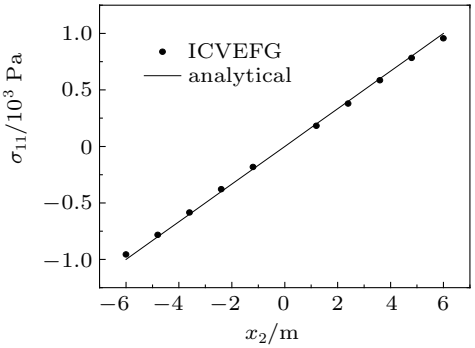


Fig. 8. Stress σ_{11} at $x_1 = L/2$.

The numerical results of the ICVEFG method are presented in Figs. 7 and 8. And it is evident that the present results are in excellent agreement with the analytical solution.

For the purpose of error estimation and convergence study, the relative error is defined as

$$r = \sum_i \left| \frac{u_i^{\text{num}} - u_i^{\text{exact}}}{u_i^{\text{exact}}} \right|^2. \tag{64}$$

For this example, the errors of the displacement under different node distributions are shown in Fig. 9. And the errors of the stress under different node distributions are shown in Fig. 10. The present results show that the more nodes there are, the greater the accuracy will be.

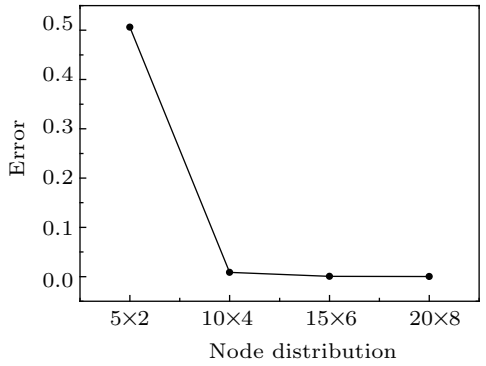


Fig. 9. Error of displacement u_2 at $x_2 = 0$.

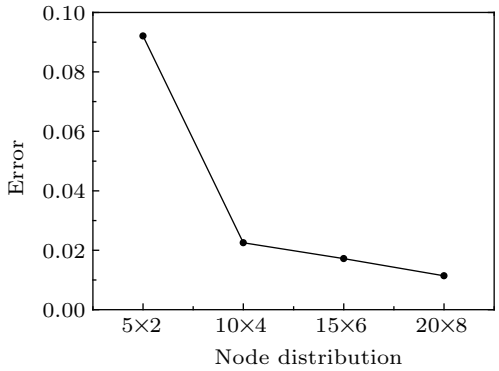


Fig. 10. Error of stress σ_{11} at $x_1 = L/2$.

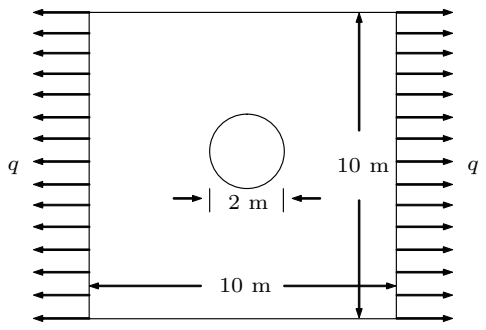


Fig. 11. A rectangular plate with a hole under a distributed load.

The second example to be considered is a perforated plate under a distributed load (see Fig. 11). The load is $p = 1000$ Pa. The other parameters that are used in our analysis are Poisson's ratio $\nu = 0.25$ and Young's modulus $E = 2.0 \times 10^8$ Pa.

The analytical displacements of this perforated rectangular plate are[19]

$$u_r = \frac{p}{4G}\Big\{r\Big[\frac{(\kappa-1)}{2} + \cos 2\theta\Big] + \frac{a^2}{r}\left[1 + (1+\kappa)\cos 2\theta\right] - \frac{a^4}{r^3}\cos 2\theta\Big\}, \quad (65)$$

$$u_\theta = \frac{p}{4G}\sin 2\theta\Big[(1-\kappa)\frac{a^2}{r} - r - \frac{a^4}{r^3}\Big], \quad (66)$$

where a is the radius of the central hole, G is the shear module, and κ is the Kolosov constant. And the corresponding analytical stresses are

$$\sigma_r = \frac{p}{2}\Big(1 - \frac{a^2}{r^2}\Big) + \frac{p}{2}\cos 2\theta\Big(1 - \frac{a^2}{r^2}\Big)\Big(1 - 3\frac{a^2}{r^2}\Big), \quad (67)$$

$$\sigma_\theta = \frac{p}{2}\Big(1 + \frac{a^2}{r^2}\Big) - \frac{p}{2}\cos 2\theta\Big(1 + 3\frac{a^4}{r^4}\Big), \quad (68)$$

$$\tau_{r\theta} = \tau_{\theta r} = -\frac{p}{2}\sin 2\theta\Big(1 - \frac{a^2}{r^2}\Big)\Big(1 + 3\frac{a^2}{r^2}\Big). \quad (69)$$

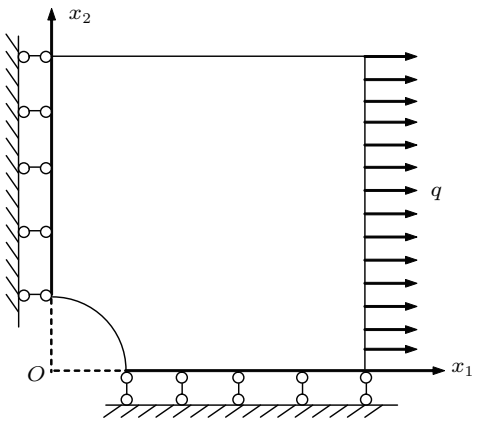


Fig. 12. A quarter of the rectangular plate and the boundary conditions.

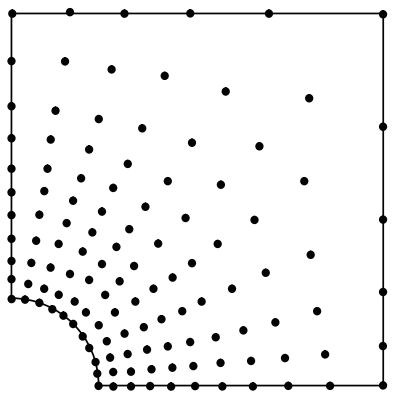


Fig. 13. Nodes in the domain of the rectangular plate with a hole.

By taking advantage of the symmetry of the model, only a quarter of the model needs to be considered in the analysis (see Fig. 12). Figure 13 shows the distribution of the nodes in the domain for this problem. The essential boundary conditions are applied with the penalty method, and the penalty factor $\alpha = 1.0 \times 10^5 E$.

The numerical results of the ICVEFG method and the CVEFG method are presented in Fig. 14, Fig. 15, and Fig. 16. And it is evident that the numerical results of displacement of the ICVEFG method and the CVEFG method are both close to the analytical solution. However the numerical results of stress of the ICVEFG method are in greater agreement with the analytical solution than the ones obtained of the CVEFG method.

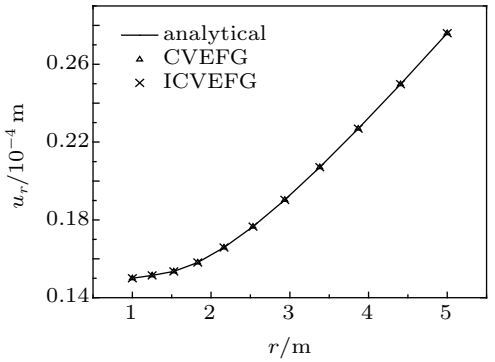


Fig. 14. Displacement u_r at $\theta = 0$.

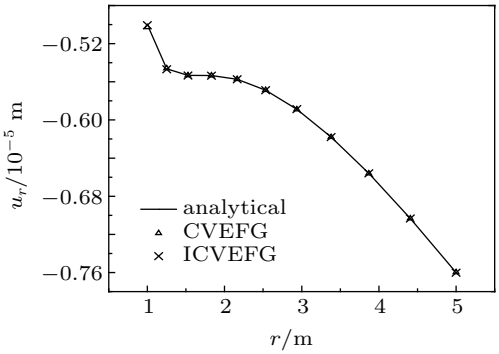


Fig. 15. Displacement u_r at $\theta = \pi/2$.

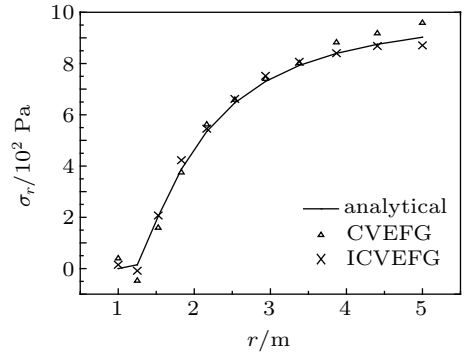


Fig. 16. Stress σ_r at $\theta = 0$.

The third example to be considered is a circular ring under a distributed inner pressure as shown in Fig. 17. The distributed inner pressure $p = 1.0 \times 10^5$, Poisson's ratio $\nu = 0.25$, and the shear module $E = 10^5$. The inner and the outer radii of the circular ring are $b = 5$ and $a = 1$ respectively.

For the plane stress case, the analytical displacements of the circular ring problem are[19]

$$u_r = \frac{a^2 pr}{E(b^2 - a^2)}\Big[1 - \nu + \frac{b^2}{r^2}(1 + \nu)\Big], \tag{70}$$

$$u_\theta = 0. \tag{71}$$

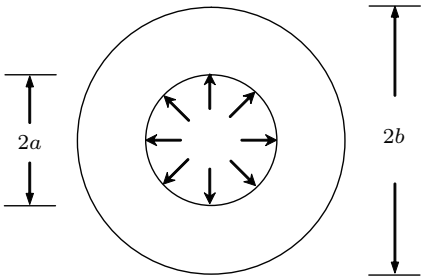


Fig. 17. A circular ring under a distributed inner pressure.

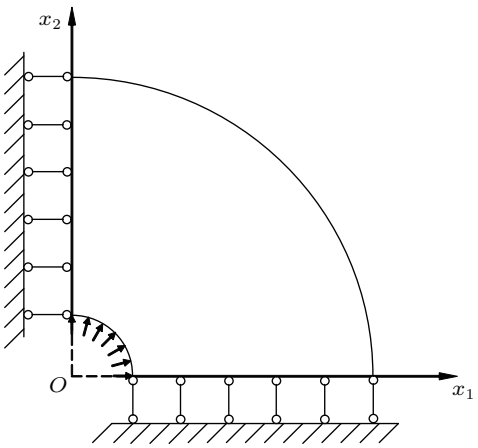


Fig. 18. Numerical model of the circular ring.

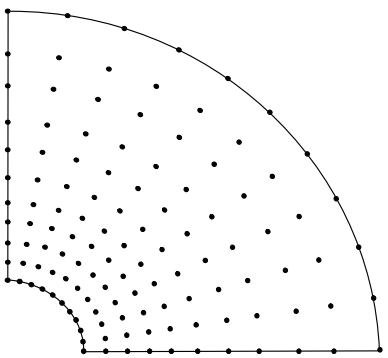


Fig. 19. Nodes in the domain of the numerical model of the circular ring.

And the corresponding stresses are

$$\sigma_r = \frac{a^2 p}{(b^2 - a^2)}\Big[1 - \frac{b^2}{r^2}\Big], \tag{72}$$

$$\sigma_\theta = \frac{a^2 p}{(b^2 - a^2)}\Big[1 + \frac{b^2}{r^2}\Big]. \tag{73}$$

By taking advantage of the symmetry of the model, only a quarter of the model needs to be considered in the analysis (see Fig. 18). Figure 19 shows the distribution of the nodes in the domain for this problem. The essential boundary conditions are applied with the penalty method, and the penalty factor $\alpha = 1.0 \times 10^2 E$.

The numerical results of the ICVEFG method are presented in Figs. 20, 21, and 22. We again verify these numerical results with the available analytical solution. As expected, it is obvious that the numerical results of the displacement of the ICVEFG method and the CVEFG method are both close to the analytical solution. However the numerical results of stress of the ICVEFG method are in much greater agreement with the analytical solution than the ones obtained of the CVEFG method.

The errors of stress varying with node distribution of the ICVEFG method and the CVEFG method are shown in Fig. 23 and Fig. 24. The present results also show that the more nodes there are, the greater the accuracy will be. It is shown that, under the same node distribution, the numerical error of the ICVEFG method is much less than that of the CVEFG method; and under the same accuracy, the ICVEFG method needs fewer nodes than the CVEFG method. The error for 8×8 node distribution of the ICVEFG is able to approach the error for 12×12 node distribution of the CVEFG method as shown in Figs. 23 and 24. The CPU time that the ICVEFG method took for 8×8 node distribution is 6.1 s, and the CPU time that the CVEFG method took for 12×12 node distribution is 34.9 s. Then the ICVEFG method has a greater computational accuracy and efficiency.

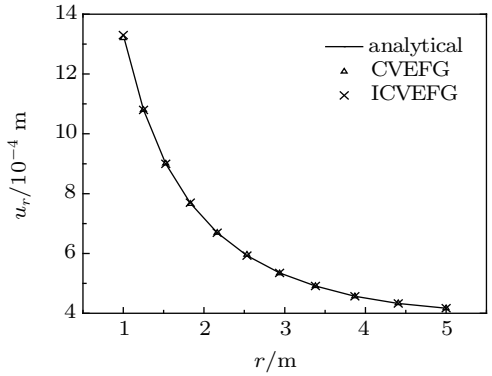


Fig. 20. Displacement u_r at $\theta = 0$.

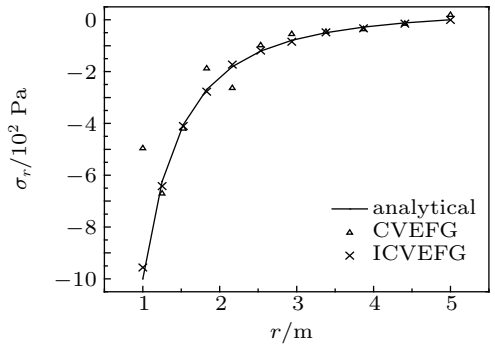


Fig.21. Stress σ_r at $\theta = 0$.

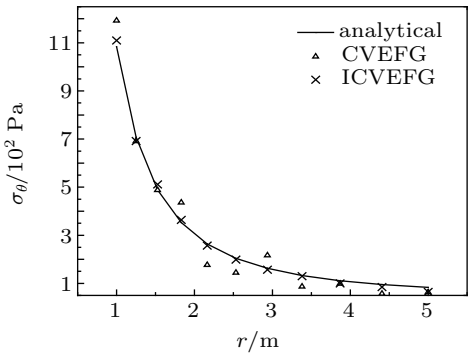


Fig.22. Stress σ_θ at $\theta = 0$.

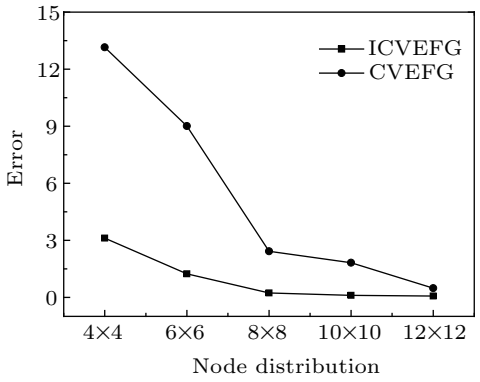


Fig.23. Error of stress σ_r at $\theta = 0$.

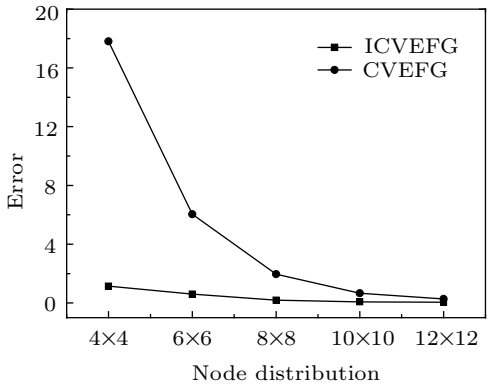


Fig.24. Error of stress σ_θ at $\theta = 0$.

5. Conclusions

In this paper, the ICVMLS approximation is presented. The ICVMLS approximation has all the advantages of the CVMLS approximation. Compared with the CVMLS approximations presented by Cheng, the functional in the ICVMLS approximation has an explicit physics meaning. Compared with the CVMLS approximations presented by Ren, the ICVMLS approximation has a greater computational accuracy and efficiency.

Based on the EFG method and the ICVMLS approximation, the ICVEFG method is presented for two-dimensional elasticity problems. Under the same node distribution, the numerical error of the ICVEFG method is much less than that of the CVEFG method. And under the same accuracy, the ICVEFG method needs fewer nodes than the CVEFG method. Thus the ICVEFG method has a greater computational accuracy and efficiency.

References

[1] Belytschko T, Krongauz Y, Organ D, Fleming M and Krysl P 1996 *Comput. Methods Appl. Mech. Engin.* **139** 3

[2] Li S C and Cheng Y M 2005 *Theor. Appl. Fracture Mech.* **44** 234

[3] Li S C, Cheng Y M and Li S C 2006 *Acta Phys. Sin.* **55** 4760 (in Chinese)

[4] Qin Y X and Cheng Y M 2006 *Acta Phys. Sin.* **55** 3215 (in Chinese)

[5] Ren H P, Cheng Y M and Zhang W 2009 *Chin. Phys.* B **18** 4065

[6] Wang J F, Bai F N and Cheng Y M 2011 *Chin. Phys.* B **20** 030206

[7] Cheng R J and Cheng Y M 2011 *Chin. Phys.* B **20** 070206

[8] Lancaster P and Salkauskas K 1981 *Math. Comput.* **37** 141

[9] Cheng Y M and Li J H 2006 *Sci. Chin. Ser.* G: *Phys. Mech. & Astron.* **49** 46

[10] Liew K M, Feng C, Cheng Y M and Kitipornchai S 2007 *Int. J. Num. Methods Engin.* **70** 46

[11] Cheng Y M, Peng M J and Li J H 2005 *Acta Mech. Sin.* **37** 719 (in Chinese)

[12] Chen L and Cheng Y M 2008 *Acta Phys. Sin.* **57** 1 (in Chinese)

[13] Chen L and Cheng Y M 2008 *Acta Phys. Sin.* **57** 6047 (in Chinese)

[14] Chen L and Cheng Y M 2010 *Chin. Phys.* B **19** 090204

[15] Cheng Y M and Li J H 2005 *Acta Phys. Sin.* **54** 4463 (in Chinese)

[16] Ren H P 2010 *Researches on the Interpolating Meshless Methods* Ph. D Thesis (Shanghai University) (in Chinese)

[17] Cheng R J and Cheng Y M 2008 *Acta Phys. Sin.* **57** 6037 (in Chinese)

[18] Cheng R J and Cheng Y M 2011 *Acta Phys. Sin.* **60** 070206 (in Chinese)

[19] Peng M J, Liu P and Cheng Y M 2009 *Int. J. Appl. Mech.* **1** 367